Atoh1 is required for the formation of lateral line electroreceptors and hair cells, whereas Foxg1 represses an electrosensory fate

Martin Minařík[1], Alexander S. Campbell[1], Roman Franěk[2#], Michaela Vazačová[2], Miloš Havelka[2], David Gela[2], Martin Pšenička[2] and Clare V. H. Baker[1]*

[1]Department of Physiology, Development & Neuroscience, University of Cambridge, Cambridge, UK
[2]Faculty of Fisheries and Protection of Waters, Research Institute of Fish Culture and Hydrobiology, University of South Bohemia in České Budějovice, Vodňany, Czech Republic

*For correspondence: cvhb1@cam.ac.uk

[#]Current address: Silberman Institute of Life Sciences, The Hebrew University of Jerusalem, Jerusalem, Israel

Abstract

In electroreceptive jawed fishes and amphibians, individual lateral line placodes form lines of neuromasts on the head containing mechanosensory hair cells, flanked by fields of ampullary organs containing electroreceptors - modified hair cells that respond to weak electric fields. Extensively shared gene expression suggests that conserved molecular mechanisms are involved in their development, but a few transcription factor genes are restricted either to the developing electrosensory or mechanosensory lateral line. Here, we used CRISPR/Cas9-mediated mutagenesis in F0-injected sterlet embryos (*Acipenser ruthenus*, a sturgeon) to test the function of three such genes. We found that the 'hair cell' transcription factor gene *Atoh1* is required for both hair cell and electroreceptor differentiation in sterlet, and for *Pou4f3* and *Gfi1* expression in both neuromasts and ampullary organs. These data support the conservation of developmental mechanisms between hair cells and electroreceptors. Targeting ampullary organ-restricted *Neurod4* did not yield any phenotype, potentially owing to redundancy with other *Neurod* genes that we found to be expressed in sterlet ampullary organs. After targeting mechanosensory-restricted *Foxg1*, ampullary organs formed within neuromast lines, suggesting that Foxg1 normally represses their development. We speculate that electrosensory organs may be the 'default' fate of lateral line primordia in electroreceptive vertebrates.

Introduction

Mechanosensory hair cells in different compartments of the inner ear transduce fluid movements for hearing and balance (Moser et al., 2020; Caprara and Peng, 2022; Mukhopadhyay and Pangrsic, 2022). In fishes and aquatic-stage amphibians, hair cells are also found in lateral line neuromasts in the skin, which are stimulated by local water movement (Mogdans, 2019; Webb, 2021). Supporting cells in neuromasts differentiate into hair cells for homeostasis and repair (Kniss et al., 2016; Lush et al., 2019) and neuromasts are easily accessible in lines over the head and trunk, making the zebrafish lateral line an excellent model for hair cell development and regeneration (Kniss et al., 2016; Nicolson, 2017; Pickett and Raible, 2019).

The lateral line system of zebrafish (a cyprinid teleost) is purely mechanosensory, as is the lateral line system of the other main anamniote lab model, the frog *Xenopus*. However, in many other vertebrates, the lateral line system also has an electrosensory division (Bullock et al., 1983; Baker et al., 2013; Crampton, 2019). In electroreceptive non-teleost jawed vertebrates, some or all of the neuromast lines on the head are flanked by fields of ampullary organs containing electroreceptors, which respond to weak cathodal stimuli such as the electric fields surrounding other animals in water (Bodznick and Montgomery, 2005; Crampton, 2019; Leitch and Julius, 2019; Chagnaud et al., 2021). Electroreception is mediated by voltage-gated calcium channels in the apical membrane (Bodznick and Montgomery, 2005; Leitch and Julius, 2019). The voltage sensor was recently identified in cartilaginous fishes as the L-type voltage-gated calcium channel $Ca_v1.3$ (Bellono et al., 2017; Bellono et al., 2018), whose pore-forming alpha subunit is encoded by *Cacna1d*. $Ca_v1.3$ is also required for synaptic transmission at hair-cell ribbon synapses (Moser et al., 2020; Mukhopadhyay and Pangrsic, 2022).

Electroreceptors, like hair cells, have an apical primary cilium and basolateral ribbon synapses with lateral line afferents (Jørgensen, 2005; Baker, 2019). However, in contrast to the highly ordered, stepped array of apical microvilli ('stereocilia') that forms the 'hair bundle' critical for hair-cell mechanotransduction (Caprara and Peng, 2022), electroreceptors in many species (e.g., cartilaginous fishes; ray-finned paddlefishes and sturgeons) lack apical microvilli altogether (Jørgensen, 2005; Baker, 2019). Electroreceptors in other species have a few apical microvilli, while the electroreceptors of the amphibian axolotl have around 200 microvilli surrounding an eccentrically positioned primary cilium (Jørgensen, 2005; Baker, 2019). Indeed, axolotl electroreceptors were described as "remarkably similar to immature hair cells" (Northcutt et al., 1994). Thus, despite their shared function, the apical surface of electroreceptors (where voltage-sensing occurs; Bodznick and Montgomery, 2005; Leitch and Julius, 2019) varies considerably across different vertebrate groups.

Fate-mapping experiments have shown that neuromasts, ampullary organs (where present) and their afferent neurons all develop from a series of pre-otic and post-otic lateral line placodes on the embryonic head (Northcutt, 1997; Piotrowski and Baker, 2014; Baker, 2019). In electroreceptive jawed vertebrates, lateral line placodes elongate to form sensory ridges that eventually fragment: neuromasts differentiate first, in a line along the centre of each ridge, and ampullary organs (if present) form later, in fields on the flanks of the ridge (Northcutt, 1997; Piotrowski and Baker, 2014; Baker, 2019). The lateral line primordia of electroreceptive vertebrates therefore provide a fascinating model for studying the formation of different sensory cell types and organs. What molecular mechanisms control the formation within the same primordium of mechanosensory neuromasts containing hair cells, versus electrosensory ampullary organs containing electroreceptors?

To gain molecular insight into electroreceptor development, we originally took a candidate-gene approach, based on genes known to be important for neuromast and/or hair cell development. This enabled us to identify a variety of genes expressed in developing ampullary organs as well as neuromasts, in embryos from the three major jawed-vertebrate groups, i.e., cartilaginous fishes (lesser-spotted catshark, *Scyliorhinus canicula*, and little skate, *Leucoraja erinacea*; O'Neill et al., 2007; Gillis et al., 2012); lobe-finned bony fishes/tetrapods (a urodele amphibian, the axolotl, *Ambystoma mexicanum*; Modrell and Baker, 2012); and ray-finned bony fishes (a chondrostean, the Mississippi paddlefish, *Polyodon spathula*; Modrell et al., 2011a; Modrell et al., 2011b; Modrell et al., 2017b). We also took an unbiased discovery approach using differential bulk RNA-seq in late-larval paddlefish, which yielded a dataset of almost 500 genes that were putatively enriched in lateral line organs (Modrell et al., 2017a). Validation by *in situ* hybridization of a subset of candidates from this dataset suggested that conserved molecular mechanisms were involved in hair cell and electroreceptor development, and that hair cells and electroreceptors were closely related physiologically (Modrell et al., 2017a). For example, developing ampullary organs express the key 'hair cell' transcription factor genes *Atoh1* and *Pou4f3* (see Roccio et al., 2020; Iyer and Groves, 2021), and genes essential for the function of hair cell ribbon synapses, including the voltage-gated calcium channel gene *Cacna1d*, encoding $Ca_v1.3$ (Modrell et al., 2017a). We also identified a handful of genes expressed in developing ampullary organs but not neuromasts, including two electroreceptor-specific voltage-gated potassium channel subunit genes (*Kcna5* and *Kcnab3*) and a single transcription factor gene, *Neurod4* (Modrell et al., 2017a).

Up to that point, we had reported the shared expression of fifteen transcription factor genes in both ampullary organs and neuromasts, but only one transcription factor gene with restricted expression, namely, electrosensory-restricted *Neurod4* (Modrell et al., 2011a; Modrell et al., 2011b; Modrell et al., 2017b). More recently (preprint: Minařík et al., 2023), we

110 used the late-larval paddlefish lateral line organ-enriched dataset (Modrell et al., 2017b), as
111 well as a candidate gene approach, to identify 23 more transcription factor genes expressed
112 within developing lateral line organs in paddlefish and/or in a related, more experimentally
113 tractable chondrostean, the sterlet (*Acipenser ruthenus*, a small sturgeon; e.g., Chen et al.,
114 2018; Baloch et al., 2019; Stundl et al., 2022). Twelve of these transcription factor genes -
115 including *Gfi1* - were expressed in both ampullary organs and neuromasts (preprint: Minařík
116 et al., 2023). Thus, developing ampullary organs, as well as neuromasts, express the three
117 'hair cell' transcription factor genes - *Atoh1*, *Pou4f3* and *Gfi1* - whose co-expression is
118 sufficient to drive postnatal mouse cochlear supporting cells to adopt a 'hair cell-like' fate, albeit
119 not to form fully mature hair cells (Roccio et al., 2020; Iyer and Groves, 2021; Chen et al.,
120 2021; Iyer et al., 2022). We also identified six novel ampullary organ-restricted transcription
121 factor genes and the first-reported mechanosensory-restricted transcription factor genes
122 (preprint: Minařík et al., 2023). One of the five mechanosensory-restricted transcription factor
123 genes was *Foxg1*, which was expressed and maintained in the central region of sensory ridges
124 where lines of neuromasts form, although excluded from hair cells (preprint: Minařík et al.,
125 2023).
126 Here, we used CRISPR/Cas9-mediated mutagenesis in F0-injected sterlet embryos to
127 investigate the function in lateral line organ development of *Atoh1*, electrosensory-restricted
128 *Neurod4* and mechanosensory-restricted *Foxg1* (for reference, Supplementary Figure S1
129 shows the normal expression patterns of these genes). We report that *Atoh1* is required for
130 the formation of electroreceptors, as well as hair cells. We did not see any phenotype after
131 targeting ampullary organ-restricted *Neurod4*, potentially owing to redundancy with other
132 *Neurod* family members that we found to be expressed in sterlet ampullary organs (and
133 neuromasts). Targeting mechanosensory-restricted *Foxg1* resulted in a striking phenotype:
134 the ectopic formation of ampullary organs within neuromast lines, and in some cases the
135 fusion of ampullary organ fields that normally develop either side of a line of neuromasts. This
136 suggests the unexpected but intriguing hypothesis that ampullary organs may be the 'default'
137 fate for lateral line sensory ridges, and that this is repressed by Foxg1, allowing neuromasts
138 to form instead.
139
140 **Results**
141
142 **CRISPR/Cas9-mediated mutagenesis in F0-injected sterlet embryos**
143 To test gene function during lateral line organ development, we optimised CRISPR/Cas9-
144 mediated mutagenesis in F0-injected sterlet embryos, building on established protocols for
145 axolotl (*Ambystoma mexicanum*; Flowers et al., 2014; Fei et al., 2018), newt (*Pleurodeles*
146 *waltl*; Elewa et al., 2017), and sea lamprey (*Petromyzon marinus*; Square et al., 2015; York et

147 al., 2019; Square et al., 2020), whose eggs are all large (1-2 mm in diameter) and easy to
148 microinject at the 1-2 cell stage. Ovulated sterlet eggs are very large: roughly 2.5 mm in
149 diameter (Lenhardt et al., 2005). (Since this project started, CRISPR/Cas9-mediated
150 mutagenesis in F0-injected sterlet embryos has been reported, including by two of us, R.F.
151 and M.P.; Chen et al., 2018; Baloch et al., 2019; Stundl et al., 2022.)

152 We targeted the melanin-producing enzyme *tyrosinase* (*Tyr*) as a positive control,
153 using eight different single-guide (sg) RNAs. Table 1 shows the sgRNA target sequences
154 (including two that were designed and recently published by Stundl et al., 2022) and the
155 various combinations in which they were injected. Supplementary Figure S2A shows the
156 position of each sgRNA relative to the exon structure of the *tyrosinase* gene. Our sgRNAs
157 were designed prior to publication of the chromosome-level sterlet genome (Du et al., 2020).
158 Searching the genome for *Tyr* showed that both *Tyr* ohnologs (i.e., gene paralogs originating
159 from the whole-genome duplication in the sterlet lineage; Du et al., 2020) have been retained,
160 on chromosomes 8 and 9, with 99.21% nucleotide identity in the coding sequence (98.81%
161 amino acid identity). However, the copy on chromosome 8 has a 7 base-pair (bp) deletion
162 (c.344_350delGAAGAGA) that would result in a frameshift early in the sequence, upstream of
163 the tyrosinase domain. Our sgRNAs target the full-length *Tyr* gene on chromosome 9. The *Tyr*
164 sgRNA 1 (Table 1; Supplementary Figure S2A) has a one-base mismatch to the *Tyr* gene on
165 chromosome 8, in position 19 of the target sequence (just 2 bp upstream of the PAM), thus
166 lying within the expected seed sequence and likely to prevent successful edits (Wu et al.,
167 2014). Nevertheless, the frameshift-causing deletion in this ohnolog suggests it does not
168 encode functional protein.

169 Three different combinations of six of the eight *Tyr* sgRNAs, when injected at the 1-2-
170 cell stage (2-4 sgRNAs pre-complexed with Cas9), each generated at least four embryos
171 (hereafter 'crispants') with pigmentation phenotypes at stage 45 (Dettlaff et al., 1993), the
172 onset of the transition to independent feeding. The other two *Tyr* sgRNAs failed to generate
173 any phenotypes (Supplementary Table 1). Excluding the *Tyr* sgRNAs that failed, at least some
174 degree of pigment loss was seen in 63/111 *Tyr* crispants (56.8%) across nine independent
175 batches. Examples of *Tyr* crispants with pigmentation phenotypes, plus a control, are shown
176 in Supplementary Figure 2B-D. The most efficient results were obtained by injecting 1-cell
177 embryos with a preassembled mix of Cas9 protein plus two chemically modified sgRNAs
178 (purchased from Synthego) against the target gene, and subsequently maintaining the
179 embryos at room temperature for around 6 hours. The time from fertilization to completion of
180 the first cleavage is around 2-3 hours at room temperature, giving plenty of time for the
181 Cas9/sgRNA complex to act before returning the embryos to colder temperatures for
182 subsequent development. (Sterlet are cold-water fish and the optimum temperature for
183 maintaining embryos for normal development is 16°C.)

Following embryo injection at the 1-2-cell stage with pre-complexed sgRNAs/Cas9 and fixation at stage 45, genomic DNA was extracted from the trunk/tail prior to analysis of the heads by *in situ* hybridization (ISH). The sgRNA-targeted region from trunk/tail genomic DNA was amplified by PCR for direct Sanger sequencing and *in silico* analysis using Synthego's online 'Inference of CRISPR Edits' (ICE) tool (Conant et al., 2022) (also see e.g., Uribe-Salazar et al., 2022) to analyse the identity and frequency of edits of the target gene. Supplementary Figure S2E-I show examples of successful disruption of *Tyr*.

We note that our genotyping results have shown that most crispants analysed, across all genes targeted, have some degree of targeted mutagenesis in the trunk/tail, with a range of deletion sizes. Although phenotypes from the initial spawning seasons were almost always highly mosaic, suggesting mutations occurred later in development, following optimization a proportion of embryos showed complete unilateral and occasionally bilateral phenotypes. Such phenotypes suggest that mutation occurred in one cell at the 2-cell stage (unilateral phenotype) or even as early as the 1-cell stage (bilateral phenotype). Some degree of mosaicism can be useful, however, as the unaffected tissue provides an internal control for the normal expression of the gene being examined by ISH.

Targeting *Atoh1* resulted in the loss of hair cells and electroreceptors

We targeted *Atoh1* for CRISPR/Cas9-mediated mutagenesis by injecting sterlet embryos at the 1-2 cell stage with Cas9 protein pre-complexed with two sgRNAs targeting *Atoh1* (Table 1; Supplementary Figure S2A). Our sgRNAs were designed prior to publication of the chromosome-level sterlet genome (Du et al., 2020). Searching the genome for *Atoh1* showed that both *Atoh1* ohnologs have been retained, on chromosomes 1 and 2, with 92.41% nucleotide identity (and 85.48% amino acid identity) in the coding sequence. The copy on chromosome 2 encodes a shorter version of the protein with a four amino acid deletion near the N-terminus (E14_G17del). Our sgRNAs target the full-length *Atoh1* gene on chromosome 1. One sgRNA has a one-base mismatch to the shorter *Atoh1* gene on chromosome 2, in position 3 of the target sequence (PAM-distal), which is unlikely to prevent successful targeting (Wu et al., 2014). Thus, we expect our sgRNAs to target both *Atoh1* ohnologs.

The *Atoh1* crispants, together with *Tyr*-targeted siblings as controls, were raised to stage 45 (the onset of independent feeding, around 14 days post-fertilization). ISH for the hair cell and electroreceptor marker *Cacna1d* (Modrell et al., 2017a) (also see preprint: Minařík et al., 2023), which was recently shown to be a direct Atoh1 target gene in mouse cochlear hair cells (Jen et al., 2022), revealed no phenotype in *Tyr* control crispants (Figure 1A-D; n=0/17 across four independent batches; Supplementary Table 1). However, *Cacna1d* expression was absent mosaically in neuromast lines and ampullary organ fields in *Atoh1* crispants (Figure 1E-J; n=13/22, i.e., 59%, across six independent batches; Supplementary Table 1).

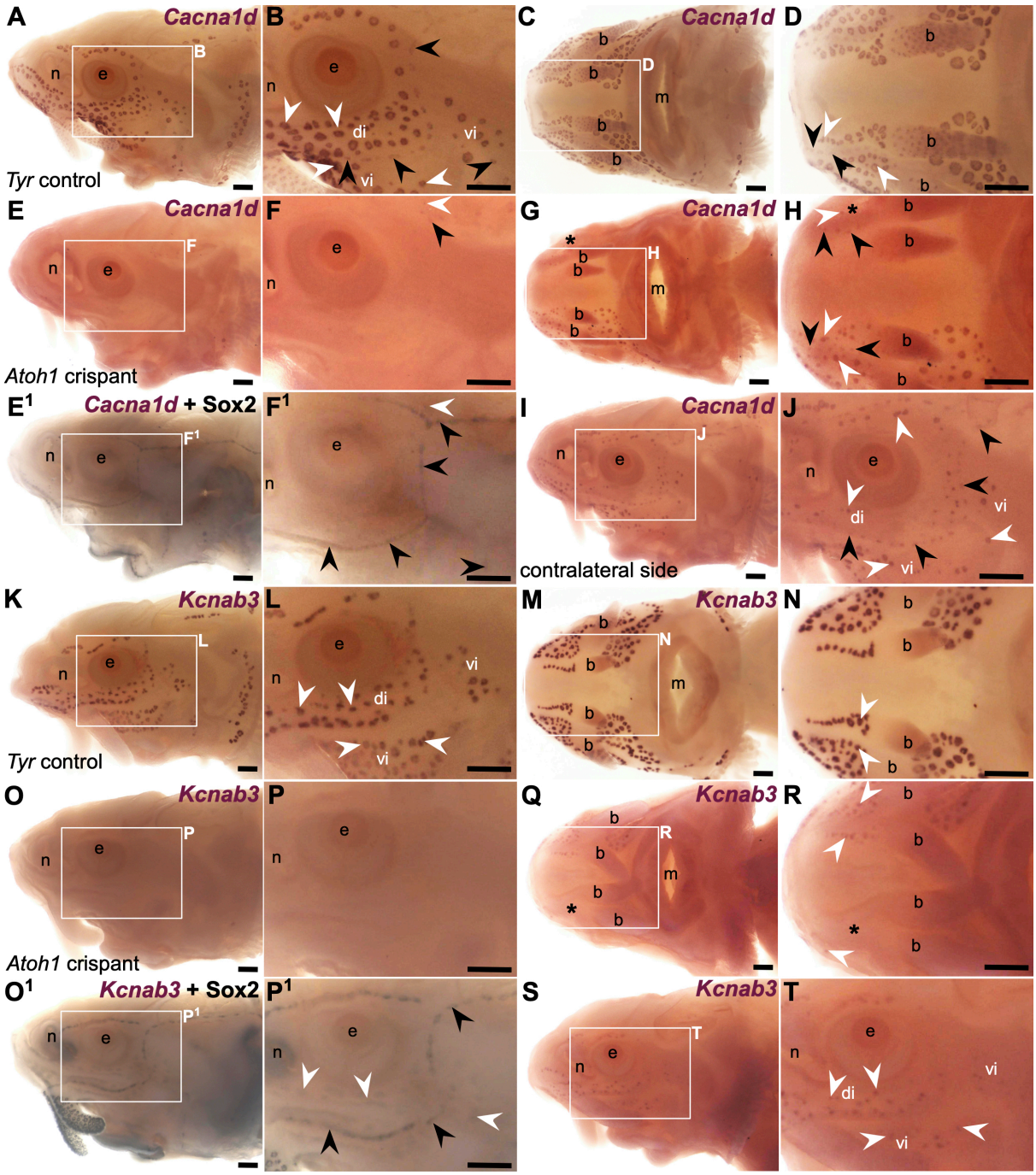

Figure 1. *Atoh1* is required for the differentiation of lateral line hair cells and electroreceptors. Sterlet crispants at stage 45 after *in situ* hybridization (ISH) for the hair cell and electroreceptor marker *Cacna1d*, or the electroreceptor-specific marker *Kcnab3*. Black arrowheads indicate examples of neuromasts; white arrowheads indicate examples of ampullary organs. (**A-D**) In a control *Tyr* crispant, *Cacna1d* expression shows the normal distribution of hair cells in lines of neuromasts, and electroreceptors in fields of ampullary organs flanking the neuromast lines (lateral view: A,B; ventral view: C,D). (**E-J**) In an *Atoh1* crispant, *Cacna1d* expression is absent on the left side of the head (E,F), except for a few isolated organs in the otic region and on the operculum. Post-ISH Sox2 immunostaining (E^1,F^1) shows that neuromast supporting cells are still present. A ventral view (G,H) and a lateral view of the right side of the head (I,J; image flipped horizontally for ease of comparison) reveal a unilateral phenotype, with *Cacna1d*-expressing hair cells and electroreceptors mostly absent from the left side only of the ventral rostrum (asterisk in G,H) and present on the right side of the head (I,J). (**K,L**) Lateral view of a control *Tyr* crispant after ISH for *Kcnab3*, showing the position of electroreceptors in ampullary organs. (**M,N**) Ventral view of another *Tyr* crispant showing *Kcnab3* expression in ampullary organs. (**O-P^1**) Lateral view of an *Atoh1* crispant in which *Kcnab3* expression is absent from ampullary organs.

Post-ISH Sox2 immunostaining (O^1,P^1) shows that supporting cells are still present in neuromasts (strong staining) and can also be detected in ampullary organs (much weaker staining). (**Q-T**) A different *Atoh1* crispant after ISH for *Kcnab3*, shown in ventral view (Q,R: compare with M,N) and lateral view (S,T). *Kcnab3* expression reveals a unilateral phenotype: *Kcnab3*-expressing electroreceptors are mostly absent from the right side (asterisk) but present on the left side. Abbreviations: b, barbel; di, dorsal infraorbital ampullary organ field; e, eye; m, mouth; n, naris; S, stage; vi, ventral infraorbital ampullary organ field. Scale bars: 200 µm.

This suggested that disruption of the *Atoh1* gene in sterlet resulted in the failure of hair cell differentiation (as expected from zebrafish; Millimaki et al., 2007) and also electroreceptors. Post-ISH immunostaining for the supporting-cell marker Sox2 (Hernández et al., 2007; Modrell et al., 2017a) (also see preprint: Minařík et al., 2023) confirmed that neuromasts had formed (Figure 1E^1,F^1), so the phenotype was specific to receptor cells. Ampullary organs were not reliably detected because Sox2 immunostaining labels neuromasts much more strongly than ampullary organs in sterlet (Supplementary Figure S1A,B; also preprint: Minařík et al., 2023), as it does in paddlefish (Modrell et al., 2017a). ISH for electroreceptor-specific *Kcnab3* (Modrell et al., 2017a) (also see preprint: Minařík et al., 2023) similarly showed no effect in *Tyr* control crispants (Figure 1K-N; n=0/27 across six independent batches; Supplementary Table 1), but the mosaic absence of *Kcnab3* expression in ampullary organ fields in *Atoh1* crispants (Figure 1O-T; n=8/13, i.e., 62%, across three independent batches; Supplementary Table 1). Post-*Kcnab3* ISH immunostaining for Sox2 confirmed that ampullary organs were still present, as well as neuromasts (Figure 1O^1,P^1).

In mouse cochlear hair cells, the 'hair cell' transcription factor genes *Pou4f3* and *Gfi1* are direct Atoh1 targets (Yu et al., 2021; Jen et al., 2022). ISH for *Pou4f3* showed no phenotype in *Tyr* controls (Figure 2A,B; n=0/9 across three batches; Supplementary Table 1) but the mosaic absence of *Pou4f3* in ampullary organ fields and neuromast lines of *Atoh1* crispants (Figure 2C-D^1; n=13/15 embryos, i.e., 87%, across three batches; Supplementary Table 1). Similarly, ISH for *Gfi1* showed no phenotype in *Tyr* controls (Figure 2E,F; n=0/17 across five batches; Supplementary Table 1), but mosaic absence of *Gfi1* in ampullary organ fields and neuromast lines of *Atoh1* crispants (Figure 2G-H^1; n=9/14 embryos, i.e., 64%, across four batches; Supplementary Table 1). Post-ISH immunostaining for Sox2 confirmed that neuromasts and ampullary organs were still present in *Atoh1* crispants (Figure 2C^1,D^1,G^1,H^1).

Genotyping and ICE analysis (Conant et al., 2022) of tails from individual *Atoh1* crispants targeted with this pair of sgRNAs, showed successful disruption of the *Atoh1* gene (Supplementary Figure S3 shows examples). Taken together, these data suggest that Atoh1 lies upstream of *Pou4f3* and *Gfi1* in ampullary organs as well as neuromasts, and is required for the differentiation of electroreceptors as well as hair cells.

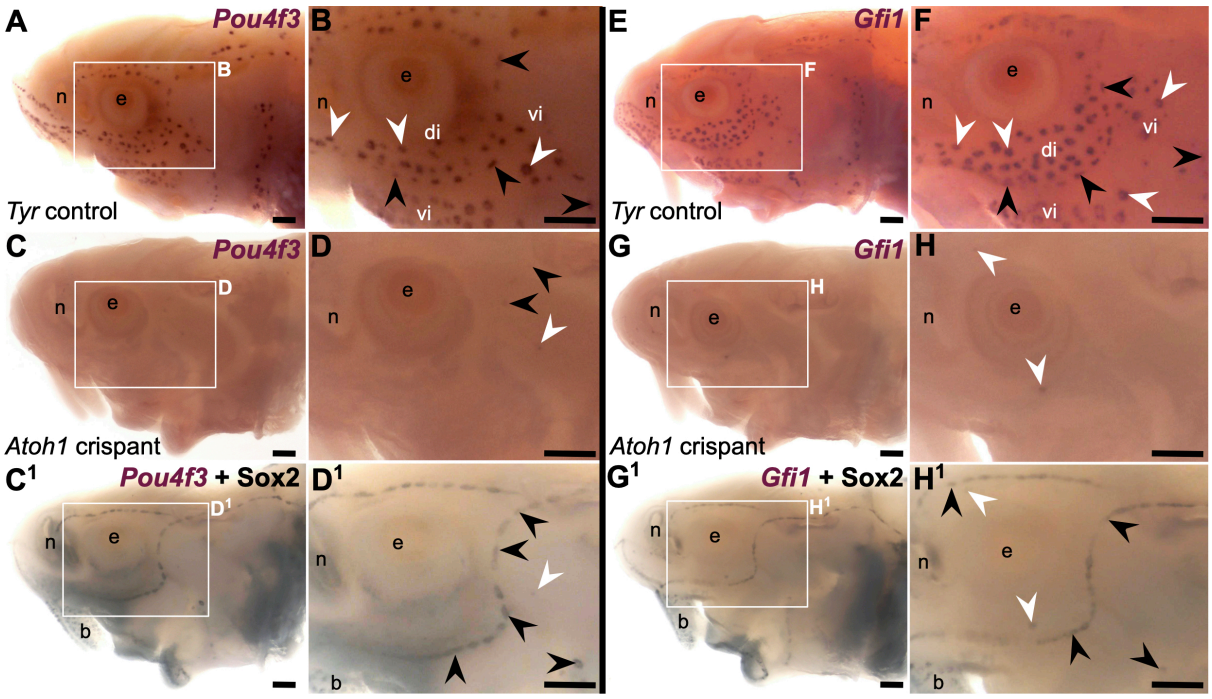

Figure 2. *Atoh1* is required for *Pou4f3* and *Gfi1* expression in ampullary organs and neuromasts. Sterlet crispants at stage 45 after *in situ* hybridization for transcription factor genes expressed by developing hair cells. Black arrowheads indicate examples of neuromasts; white arrowheads indicate examples of ampullary organs. (**A,B**) In a control *Tyr* crispant, *Pou4f3* expression is detected in both neuromasts and ampullary organs. (**C-D^1**) In an *Atoh1* crispant, *Pou4f3* expression is absent from both neuromasts and ampullary organs, except for a few isolated organs in the postorbital region. Post-ISH Sox2 immunostaining (C^1,D^1) shows that neuromast supporting cells are still present. Most ampullary organs are not visible as Sox2 expression in ampullary organs is significantly weaker than in neuromasts (Supplementary Figure S1A,B) and often not detectable after post-ISH immunostaining. (**E,F**) In a control *Tyr* crispant, *Gfi1* expression is detected in both neuromasts and ampullary organs. (**G-H^1**) In an *Atoh1* crispant, *Gfi1* expression is absent from both neuromasts and ampullary organs, except for a few isolated organs in the supra- and infraorbital region. Post-ISH Sox2 immunostaining (G^1,H^1) shows that neuromast supporting cells are still present. (Most ampullary organs are not visible due to weaker Sox2 immunostaining.) Abbreviations: b, barbel; di, dorsal infraorbital ampullary organ field; e, eye; n, naris; S, stage; vi, ventral infraorbital ampullary organ field. Scale bars: 200 µm.

Targeting electrosensory-restricted *Neurod4* had no obvious effect

We previously identified *Neurod4* in paddlefish as the first-reported ampullary organ-restricted transcription factor in the developing lateral line system (Modrell et al., 2017a). We confirmed that sterlet *Neurod4* is similarly expressed by ampullary organs but not neuromasts (Supplementary Figure S1I,J). We targeted *Neurod4* in sterlet embryos using nine different sgRNAs (Table 1; Supplementary Figure S4A), injected in eight different combinations of 1-4 different sgRNAs across 10 independent batches of 1-2 cell-stage embryos (Supplementary Table 1). This had no detectable effect on expression of electroreceptor-specific *Kcnab3* (n=0/44 across nine batches, Supplementary Table 1) or the hair cell/electroreceptor marker *Cacna1d* (n=0/4 across two batches, Supplementary Table 1). Examples of *Neurod4* crispants after ISH for *Kcnab3*, plus a *Tyr* control crispant for comparison, are shown in Supplementary Figure S4B-D. Our sgRNAs were designed prior to publication of the chromosome-level sterlet

genome (Du et al., 2020). Surprisingly, we were unable to find *Neurod4* by BLAST search of the published genome. However, a single copy of *Neurod4* is annotated in the independent Vertebrate Genomes Project paternal haplotype genome assembly (publicly available via the Ensembl Rapid Release website; https://rapid.ensembl.org/Acipenser_ruthenus_GCA_902713435.1), with a prediction score of 99.96% (ENSARTG00010019470.1). This is also a match for the *Neurod4* sequence from our *de novo*-assembled sterlet transcriptome and the cDNA fragment cloned from this. Therefore, it seems that only one copy of *Neurod4* has been retained in the sterlet genome. Genotyping and ICE analysis (Conant et al., 2022) showed successful disruption of the *Neurod4* gene arising from six different combinations of the sgRNAs (Supplementary Table 1; examples are shown in Supplementary Figure S4E-I). Not all sgRNA combinations were genotyped, but all *Neurod4* crispants counted (n=44) included at least one sgRNA confirmed to disrupt the *Neurod4* gene via genotyping of other embryos (Supplementary Table 1).

The lack of phenotype in *Neurod4* crispants, despite successful disruption of the *Neurod4* gene, suggested either that Neurod4 is not required for electroreceptor differentiation, despite its restriction to ampullary organs in both paddlefish and sterlet (Modrell et al., 2017a; this paper), or that it acts redundantly with other transcription factors. In paddlefish, *Neurod1* expression was restricted to developing lateral line ganglia (Modrell et al., 2011b). We cloned sterlet *Neurod1*, *Neurod2* and *Neurod6*. (Unlike *Neurod4*, these three *Neurod* family members are all direct Atoh1 targets in mouse hair cells; Jen et al., 2022.) These three genes all proved to be expressed in sterlet ampullary organs, as well as neuromasts (Supplementary Figure S5). Thus, it seems likely that the lack of effect of CRISPR/Cas9-mediated targeting of sterlet *Neurod4* is due to redundancy with other Neurod family transcription factors co-expressed in ampullary organs. (Our results also show there is at least some variation in *Neurod* family gene expression within the developing lateral line systems of paddlefish and sterlet.)

Targeting mechanosensory-restricted *Foxg1* led to the formation of ectopic ampullary organs within neuromast lines

We recently identified *Foxg1* as a mechanosensory lateral line-restricted transcription factor gene in paddlefish and sterlet (preprint: Minařík et al., 2023). *Foxg1* is expressed in the central zones of lateral line sensory ridges where neuromasts form, though excluded from hair cells themselves (preprint: Minařík et al., 2023). Our sgRNAs against *Foxg1* (Table 1; Supplementary Figure S6A) were designed prior to publication of the chromosome-level sterlet genome (Du et al., 2020). Searching the genome for *Foxg1* showed that both *Foxg1* ohnologs have been retained, on chromosomes 16 and 24, with 99.35% nucleotide identity in

342 the coding sequence (99.51% amino acid identity). Our sgRNAs target both *Foxg1* ohnologs
343 without mismatches.

344 When compared with *Tyr* control crispants (Figure 3A-D), a striking phenotype was
345 seen mosaically after targeting mechanosensory-restricted *Foxg1* with sgRNAs 1 and 2 (Table
346 1; Supplementary Figure S6A): neuromast lines were often interrupted by ectopic ampullary
347 organs. These were defined as *Cacna1d*-expressing cells present within neuromast lines in
348 larger clusters than expected for neuromasts, resembling ampullary organs (Figure 3E-L;
349 n=9/18, i.e., 50%, across two independent batches; Supplementary Table 1), or by expression
350 of electroreceptor-specific *Kcnab3* within neuromast lines, not seen in *Tyr* control crispants
351 (Figure 3M-V; n=7/24, i.e., 29%, across both batches; Supplementary Table 1). This
352 sometimes led to the apparent fusion of ampullary organ fields across a missing neuromast
353 line (e.g., Figure 3E-H,S-V). Post-*Kcnab3* ISH immunostaining for Sox2, to reveal neuromasts,
354 also confirmed that the ectopic electroreceptors in *Foxg1* crispants were within neuromast
355 lines (Figure 3Q[1],R[1]). Targeting *Foxg1* with a different pair of sgRNAs (Table 1;
356 Supplementary Figure 6A) in a different batch of embryos generated similar phenotypes in
357 3/21 embryos (14%) overall (*Cacna1d*: n=1/6, i.e., 17%; *Kcnab3*: n=2/15, i.e., 13%;
358 Supplementary Table 1).

359 We also investigated this phenotype by performing ISH for two ampullary organ-
360 restricted transcription factor genes, *Mafa* (preprint: Minařík et al., 2023) and *Neurod4* (Modrell
361 et al., 2017a; this study), followed by Sox2 immunostaining in some embryos to reveal the
362 location of neuromasts. Relative to the normal ampullary organ expression of *Mafa* in
363 uninjected siblings (sufficient *Tyr* control crispants were not available to test; Figure 4A-D;
364 n=0/6 within one batch), ISH for *Mafa* showed the mosaic presence of ampullary organs in
365 neuromast lines and/or merging of ampullary organ fields in *Foxg1* crispants (Figure 4E-J;
366 n=3/17 embryos i.e., 18%, across two independent batches; Supplementary Table 1).
367 Similarly, relative to the usual ampullary organ expression of *Neurod4* in uninjected siblings
368 (sufficient *Tyr* control crispants were not available to test; Figure 4K-N; n=0/2 embryos within
369 one batch; Supplementary Table 1), ISH for *Neurod4* (more weakly expressed than *Mafa*)
370 revealed the same ectopic ampullary organ phenotype in *Foxg1* crispants as seen for
371 *Cacna1d*, *Kcnab3* and *Mafa* (Figure 4O-T; n=3/6 embryos, i.e., 50%, within one batch;
372 Supplementary Table 1). Genotyping and ICE analysis (Conant et al., 2022) of tails from
373 individual *Foxg1* crispants showed successful disruption of the *Foxg1* gene (Supplementary
374 Figure S6 shows examples). Overall, these data suggest that mechanosensory-restricted
375 Foxg1 acts to repress the formation of ampullary organs and electroreceptors within
376 neuromast lines.

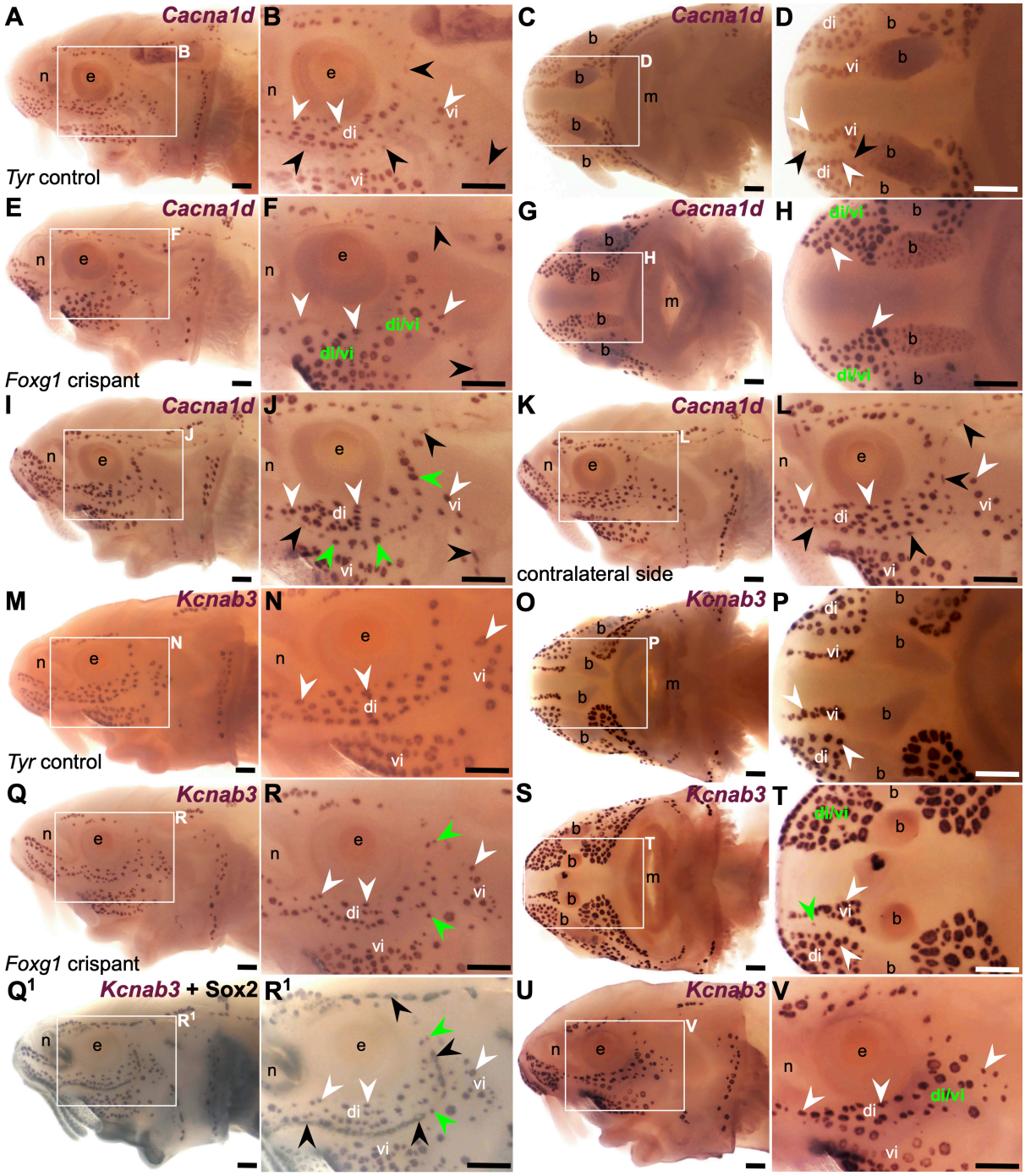

Figure 3. *Foxg1* represses ampullary organ and electroreceptor formation within neuromast lines. Sterlet crispants at stage 45 after *in situ* hybridization (ISH) for the hair cell and electroreceptor marker *Cacna1d*, or the electroreceptor-specific marker *Kcnab3*. Black arrowheads indicate examples of neuromasts; white arrowheads indicate examples of ampullary organs. (**A,B**) Lateral view of a control *Tyr* crispant. *Cacna1d* expression shows the normal distribution of hair cells and electroreceptors. Note that ampullary organs have significantly more *Cacna1d*-expressing receptor cells than neuromasts. (**C,D**) Ventral view of a second control *Tyr* crispant. *Cacna1d* expression reveals the infraorbital neuromast line on both sides of the ventral rostrum, flanked by the dorsal infraorbital (di) and ventral infraorbital (vi) ampullary organ fields. (**E,F**) Lateral view of a *Foxg1* crispant. *Cacna1d* expression reveals that distinct neuromast lines are missing and the corresponding space is filled by putative ectopic ampullary organs, based on the large, ampullary organ-like clusters of *Cacna1d*-expressing cells. The dorsal and ventral infraorbital ampullary organ fields seem to have fused across the missing neuromast line (compare with A,B). (**G,H**) Ventral view of a second *Foxg1* crispant. *Cacna1d* expression reveals an apparent fusion of the dorsal infraorbital (di) and ventral infraorbital (vi) ampullary organ

fields across the missing infraorbital neuromast lines on both sides (compare with C,D). (**I-K**) In a third *Foxg1* crispant, *Cacna1d* expression on the left side (I,J) shows that distinct supraorbital and infraorbital neuromast lines are still present. However, some organs within the supraorbital line and most organs within the infraorbital line have large clusters of *Cacna1d*-expressing cells, suggesting they are ectopic ampullary organs (green arrowheads in J show examples). On the right side (K,L; image flipped horizontally for ease of comparison), this phenotype is not seen. (**M,N**) Lateral view of a third control *Tyr* crispant. Electroreceptor-specific *Kcnab3* expression shows the distribution of ampullary organs only. (**O,P**) Ventral view of a fourth control *Tyr* crispant. *Kcnab3* expression shows the distribution of ampullary organ fields. Note the lack of staining where the infraorbital neuromast lines run on either side of the ventral rostrum, flanked by the dorsal infraorbital (di) and ventral infraorbital (vi) ampullary organ fields (compare with *Cacna1d* expression in C,D). (**Q-R^1**) Lateral view of a fourth *Foxg1* crispant. *Kcnab3* expression shows two ectopic ampullary organs (green arrowheads) within the infraorbital neuromast line (compare with M,N). Post-ISH Sox2 immunostaining for supporting cells (Q^1,R^1) confirms the position of the neuromast lines. (**S,T**) Ventral view of a fifth *Foxg1* crispant. On the left side, ectopic *Kcnab3*-expressing electroreceptors fill the space where the left infraorbital neuromast line would normally run, such that the dorsal and ventral infraorbital ampullary organ fields seem to have fused (compare with O,P). On the right side, a single ectopic *Kcnab3*-expressing ampullary organ is visible (green arrowhead) where the right infraorbital neuromast line runs (compare with O,P). (**U,V**) Lateral view of a sixth *Foxg1* crispant. *Kcnab3* expression shows fusion of the dorsal infraorbital ampullary organ field with the dorsal part of the ventral infraorbital ampullary organ field (compare with M,N). Abbreviations: b, barbel; di, dorsal infraorbital ampullary organ field; di/vi, fused dorsal infraorbital and ventral infraorbital ampullary organ fields; e, eye; m, mouth; n, naris; S, stage; vi, ventral infraorbital ampullary organ field. Scale bars: 200 µm.

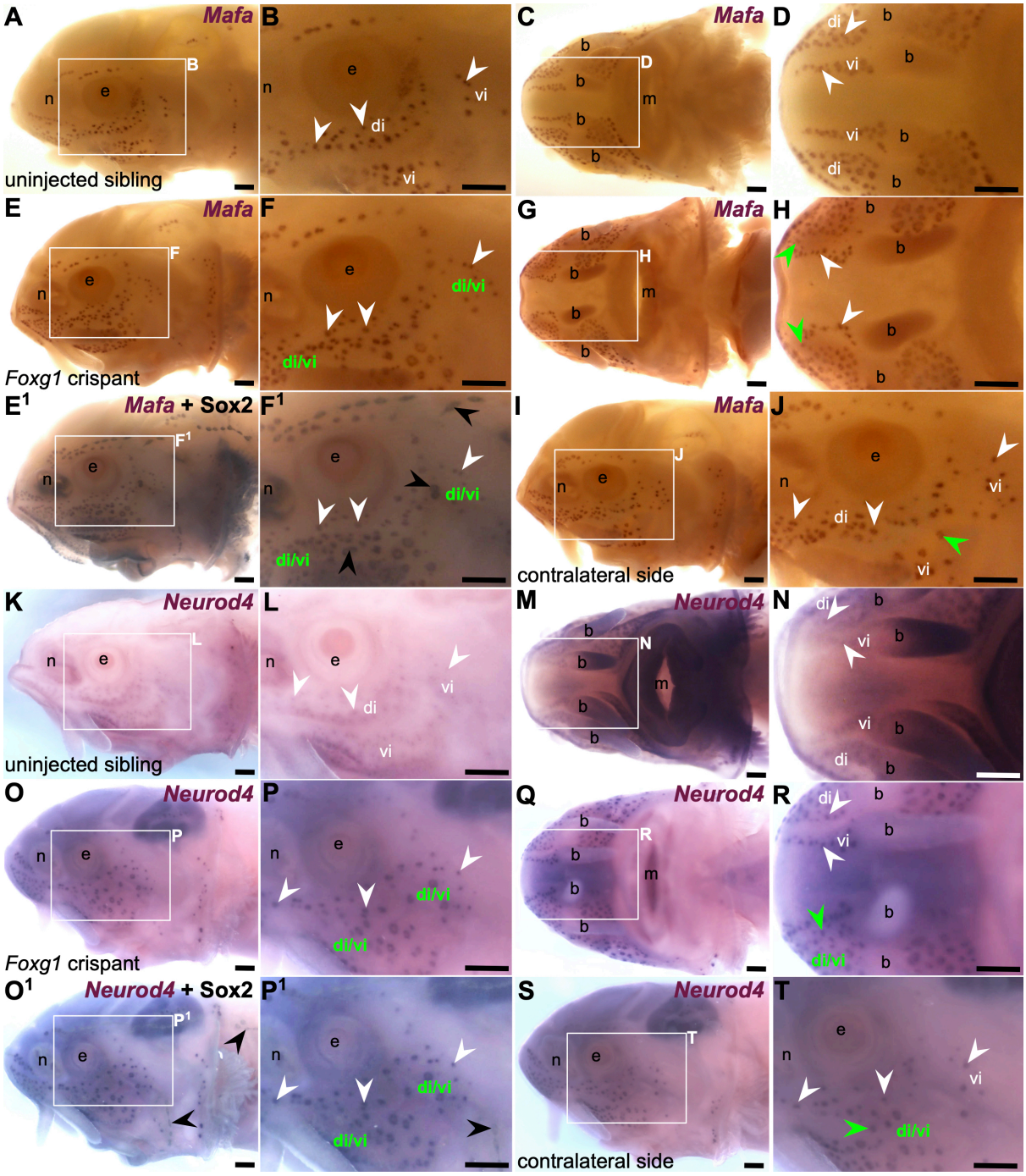

Figure 4. Ectopic ampullary organs in *Foxg1* crispants express ampullary organ-specific transcription factor genes *Mafa* and *Neurod4*. Sterlet crispants at stage 45 after *in situ* hybridization (ISH) for ampullary organ-restricted transcription factor genes. Black arrowheads indicate examples of neuromasts; white arrowheads indicate examples of ampullary organs. (**A-D**) In an uninjected sibling, *Mafa* expression is restricted to ampullary organs (lateral view: A,B; ventral view: C,D). (**E-J**) A *Foxg1* crispant. On the left side of the head (E,F), several *Mafa*-expressing ectopic ampullary organs are present in the space where the infraorbital neuromast line would normally run, such that the dorsal and ventral infraorbital ampullary organ fields seem to have fused (compare with A,B). Post-ISH Sox2 immunostaining (E^1,F^1) shows that neuromasts are still present both proximally and distally to the sites of ampullary organ field fusion. In ventral view (G,H), ectopic ampullary organs (green arrowheads) are seen bilaterally, within the spaces where the infraorbital neuromast lines run on either side of the ventral rostrum (compare with C,D). On the right side in lateral view (I,J; image flipped horizontally for ease of comparison), a single *Mafa*-expressing ectopic ampullary organ (green arrowhead) is also present in the space where the infraorbital neuromast line runs (compare with A,B). (**K-N**) In an uninjected sibling,

Neurod4 expression is restricted to ampullary organs (lateral view: K,L; ventral view: M,N). (**O-T**) A *Foxg1* crispant. On the left side of the head (O,P), *Neurod4*-expressing ectopic ampullary organs are present in the space where the infraorbital neuromast line would normally run, such that the dorsal and ventral infraorbital ampullary organ fields seem to have fused (compare with K,L). Post-ISH Sox2 immunostaining (O^1,P^1) suggests that neuromasts are absent from the site of infraorbital ampullary organ field fusion, although neuromasts can be seen in the preopercular and trunk lines (black arrowheads, compare with O,P). In ventral view (Q,R), ectopic *Neurod4*-expressing ampullary organs are seen where the right infraorbital neuromast line would normally run on the ventral rostrum (green arrowhead indicates an example), resulting in partial fusion of the dorsal and ventral infraorbital fields on this side (the left side is unaffected). On the right side in lateral view (S,T; image flipped horizontally for ease of comparison), ectopic ampullary organs are also present in the space where the infraorbital neuromast line runs (green arrowhead in T indicates an example), resulting in the apparent partial fusion of the dorsal and ventral infraorbital ampullary organ fields (compare with K,L). Abbreviations: b, barbel; di, dorsal infraorbital ampullary organ field; di/vi, fused dorsal infraorbital and ventral infraorbital ampullary organ fields; e, eye; m, mouth; n, naris; S, stage; vi, ventral infraorbital ampullary organ field. Scale bars: 200 µm.

Discussion

Conserved molecular mechanisms underlie lateral line electroreceptor and hair cell formation

Here, we aimed to test the function in lateral line electroreceptor and/or hair cell formation of three transcription factor genes that we had previously identified as expressed in developing electrosensory ampullary organ and/or mechanosensory lateral line organs in ray-finned chondrostean fishes - paddlefish and sterlet (Butts et al., 2014; Modrell et al., 2017a; preprint: Minařík et al., 2023). The first gene we investigated was *Atoh1*, which is required for the formation of lateral line hair cells in zebrafish (Millimaki et al., 2007), as well as hair cells in the inner ear (Bermingham et al., 1999; Millimaki et al., 2007). In paddlefish (Butts et al., 2014; Modrell et al., 2017a) and sterlet (preprint: Minařík et al., 2023), *Atoh1* is expressed in ampullary organs as well as neuromasts. Targeting *Atoh1* for CRISPR/Cas9-mediated mutagenesis in F0 sterlet embryos showed that Atoh1 is required for the formation not only of *Cacna1d*-expressing neuromast hair cells, as expected from zebrafish (Millimaki et al., 2007), but also of *Cacna1d*-expressing, *Kcnab3*-expressing electroreceptors. These experiments also showed that Atoh1 is required for the expression of the 'hair cell' transcription factor genes *Gfi1* and *Pou4f3* in developing ampullary organs, as well as neuromasts. This is consistent with both of these genes being direct Atoh1 targets in mouse cochlear hair cells (Yu et al., 2021; Jen et al., 2022).

In both inner-ear hair cells and Merkel cells (epidermal mechanoreceptors found in all vertebrates; see e.g., Whitear, 1989; Brown et al., 2023), Atoh1 acts with Pou4f3 in a conserved 'feed-forward circuit', with Atoh1 directly activating *Pou4f3* expression, and Pou4f3 then acting as a pioneer factor to open a significant subset of Atoh1 target enhancers (some shared and some divergent between hair cells and Merkel cells), enabling mechanosensory

differentiation (Yu et al., 2021). In hair cells, *Gfi1* is one of the Pou4f3-dependent Atoh1 targets (Yu et al., 2021). Together with the striking conservation of transcription factor gene expression between developing ampullary organs and neuromasts (Modrell et al., 2011b; Modrell et al., 2011a; Modrell et al., 2017b; Modrell et al., 2017a; preprint: Minařík et al., 2023), the phenotypes seen in *Atoh1*-targeted F0 sterlet crispant embryos suggest that the molecular mechanisms underlying electroreceptor formation are highly conserved with those underlying hair cell formation. Indeed, the requirement of Atoh1 for *Pou4f3* and *Gfi1* expression in ampullary organs, as well as neuromasts, suggests that the Atoh1-Pou4f3 'feedforward circuit' in mechanosensory cells - i.e., hair cells and epidermal Merkel cells (Yu et al., 2021) - may also be conserved, at least partly, in developing electroreceptors. Taken together, these data support the hypothesis that electroreceptors evolved as a transcriptionally related "sister cell type" to lateral line hair cells (Arendt et al., 2016; Baker and Modrell, 2018; Baker, 2019).

Electrosensory-restricted Neurod4 is likely redundant with other Neurod family members in sterlet

Paddlefish *Neurod4* was the first-reported ampullary organ-restricted transcription factor gene (Modrell et al., 2017a), with conserved expression in sterlet (this study). We were unable to detect a lateral line organ phenotype in *Neurod4*-targeted sterlet crispants. However, we found that *Neurod1*, *Neurod2* and *Neurod6* are all expressed in sterlet ampullary organs (as well as neuromasts), suggesting that Neurod4 may act redundantly with one or more of these factors in developing ampullary organs. (In paddlefish, however, *Neurod1* expression is restricted to developing lateral line ganglia; Modrell et al., 2011b.) Targeting multiple *Neurod* genes for CRISPR/Cas9-mediated mutagenesis in the future may shed light on the role played by this transcription factor family in ampullary organ development.

Foxg1 represses electroreceptor formation in the neuromast-forming central zone of lateral line sensory ridges

We also targeted *Foxg1*, a mechanosensory-restricted transcription factor gene that we recently identified in the developing lateral line system of paddlefish and sterlet (preprint: Minařík et al., 2023). *Foxg1* is expressed in the central zones of lateral line sensory ridges where neuromasts form, though excluded from the central domains of neuromasts where hair cells differentiate (preprint: Minařík et al., 2023). Targeting *Foxg1* for CRISPR/Cas9-mediated mutagenesis in F0 sterlet embryos led to a striking phenotype: the formation within neuromast lines of ectopic electroreceptors, often in the large clusters normally seen in ampullary organs. In some cases, ampullary organ fields, which normally flank neuromast lines, effectively 'merged' across missing neuromast lines. This phenotype was revealed by examining expression of the electroreceptor-specific marker *Kcnab3*, and two ampullary organ-restricted

510 transcription factor genes: *Mafa* (preprint: Minařík et al., 2023) and *Neurod4* (Modrell et al.,
511 2017a). Thus, *Foxg1* seems to repress an ampullary organ fate within the central domain of
512 lateral line sensory ridges where neuromasts form.

513 In the mouse inner ear, *Foxg1* is expressed in the prospective cochlea and all sensory
514 patches, in hair cell progenitors and supporting cells (Pauley et al., 2006; Tasdemir-Yilmaz et
515 al., 2021), plus a subset of hair cells (Pauley et al., 2006). Knockout leads to a shorter cochlea
516 with extra rows of hair cells, and to loss or reduction of vestibular end organs (Pauley et al.,
517 2006; Hwang et al., 2009). More hair cells and fewer supporting cells were seen after
518 conditional knockdown of *Foxg1* in neonatal cochlear supporting cells, possibly via the
519 transdifferentiation of supporting cells (Zhang et al., 2019; Zhang et al., 2020). This suggests
520 the possibility that Foxg1 may act in the central zone of lateral line sensory ridges to maintain
521 a proliferative progenitor state, as it does in the mouse olfactory epithelium (Kawauchi et al.,
522 2009).

523 Furthermore, Fox family members can act as pioneer factors as well as transcription
524 factors (Golson and Kaestner, 2016; Lukoseviciute et al., 2018). A pioneer factor role has
525 been proposed for Foxi3 in otic placode development (see Singh and Groves, 2016). In the
526 developing neural crest, Foxd3 acts early as a pioneer factor, opening enhancers and
527 repositioning nucleosomes to prime genes controlling neural crest specification and migration
528 and, concurrently, to repress the premature differentiation of, e.g., melanocytes (Lukoseviciute
529 et al., 2018). Later in neural crest development, Foxd3 represses enhancers associated with
530 mesenchymal, neuronal and melanocyte lineages (Lukoseviciute et al., 2018). In cortical
531 progenitors, Foxg1 suppresses the adoption at later stages of an early-born cell fate, namely,
532 Cajal-Retzius cells (Hanashima et al., 2004). In the developing chicken otic placode, Foxg1
533 represses markers of other lineages, such as the olfactory and lens placodes, and epidermis
534 (Anwar et al., 2017). Hence, it is possible that Foxg1 acts in the central zone of lateral line
535 sensory ridges in electroreceptive fishes as a pioneer factor for neuromast/hair cell formation,
536 and/or that it represses ampullary organ/electroreceptor formation. Such a role would be
537 consistent with lateral line expression of *Foxg1* only in electroreceptive fishes: *Foxg1* is not
538 expressed in the developing lateral line of zebrafish or *Xenopus* (e.g., Dirksen and Jamrich,
539 1995; Papalopulu and Kintner, 1996; Toresson et al., 1998; Eagleson and Dempewolf, 2002;
540 Duggan et al., 2008; Zhao et al., 2009).

541 Overall, these data lead us to propose the speculative hypothesis that electrosensory
542 organs may be the 'default' fate within lateral line sensory ridges in electroreceptive
543 vertebrates, and that Foxg1 represses this fate to enable mechanosensory neuromasts and
544 hair cells to form. To test these hypotheses directly, it will be important in the future to identify
545 global changes in gene expression and chromatin accessibility in the absence of Foxg1.
546

547 **Summary and Perspective**

548 Overall, we have found that the 'hair cell' transcription factor Atoh1 is required for the formation
549 of lateral line electroreceptors as well as hair cells, consistent with a close developmental
550 relationship between these putative 'sister cell' types. Electrosensory-restricted Neurod4 may
551 act redundantly with other Neurod family members expressed in developing ampullary organs.
552 Mechanosensory-restricted Foxg1 represses the formation of electroreceptors within
553 neuromast lines, suggesting the surprising possibility that electroreceptors are the 'default'
554 fate within lateral line sensory ridges and raising interesting developmental and evolutionary
555 questions for future investigation.

556

557 **Materials and Methods**

558

559 **Animals**

560 Fertilized sterlet (*Acipenser ruthenus*) eggs were obtained from the breeding facility at the
561 Research Institute of Fish Culture and Hydrobiology, Faculty of Fisheries and Protection of
562 Waters, University of South Bohemia in České Budějovice, Vodňany, Czech Republic, and
563 staged according to Dettlaff et al. (1993). For detailed information about sterlet husbandry, *in*
564 *vitro* fertilization and the rearing of embryos and yolk-sac larvae, see Stundl et al. (2022). Upon
565 reaching the desired developmental stages, embryos and yolk-sac larvae were euthanized by
566 overdose of MS-222 (Sigma-Aldrich) and fixed in modified Carnoy's fixative (6 volumes 100%
567 ethanol: 3 volumes 37% formaldehyde: 1 volume glacial acetic acid) for 3 hours at room
568 temperature, dehydrated stepwise into 100% ethanol and stored at -20°C.

569 All experimental procedures were approved by the Animal Research Committee of the
570 Faculty of Fisheries and Protection of Waters in Vodňany, University of South Bohemia in
571 České Budějovice, Czech Republic, and by the Ministry of Agriculture of the Czech Republic
572 (reference number: MSMT-12550/2016-3). Experimental fish were maintained according to
573 the principles of the European Union (EU) Harmonized Animal Welfare Act of the Czech
574 Republic, and Principles of Laboratory Animal Care and National Laws 246/1992 "Animal
575 Welfare" on the protection of animals.

576

577 **CRISPR guide RNA design and synthesis**

578 Target gene sequences were identified using the National Center for Biotechnology
579 Information (NCBI) Basic Local Alignment Search Tool BLAST
580 (https://blast.ncbi.nlm.nih.gov/Blast.cgi; McGinnis and Madden, 2004) to search sterlet
581 transcriptomic data (available at DDBJ/EMBL/GenBank under the accessions
582 GKLU00000000 and GKEF01000000; see preprint: Minařík et al., 2023) or draft genomic
583 sequence data (M.H., unpublished) with the relevant paddlefish sequence (Modrell et al.,

584 2017a). Transcriptomic sequence data were searched for *Tyr*, *Atoh1* and *Neurod4*; genomic
585 sequence data were searched for *Foxg1*. Since the project started, a chromosome-level sterlet
586 genome has been published (Du et al., 2020) and an independent high-quality genome
587 assembly from the Vertebrate Genomes Project has been made publicly available at
588 RapidEnsembl (https://rapid.ensembl.org/Acipenser_ruthenus_GCA_902713435.1). Open
589 reading frames were identified using the NCBI ORF Finder tool
590 (https://www.ncbi.nlm.nih.gov/orffinder/) and exons annotated by comparison with reference
591 anamniote species (*Lepisosteus oculatus*, *Danio rerio*, *Xenopus tropicalis*) available via
592 Ensembl (https://www.ensembl.org; Cunningham et al., 2022). Conserved domains were
593 identified using NCBI BLASTX (https://blast.ncbi.nlm.nih.gov/Blast.cgi; McGinnis and
594 Madden, 2004). gRNAs were preferentially designed to target 5' exons, ideally upstream of or
595 within regions encoding known functional domains, to increase the probability of disrupting
596 gene function. gRNAs were designed using the CRISPR Guide RNA Design Tool from
597 Benchling (https://benchling.com) and selected for synthesis based on the following criteria:
598 (1) a high on-target score, ideally no less than 0.5; (2) no off-target matches identified within
599 coding sequences in transcriptome and genome data, unless there were at least two
600 mismatches in the 3' seed sequence (8-10 bp upstream of the protospacer adjacent motif
601 [PAM], or in the PAM itself); (3) if multiplexing, the gRNA pair were ideally within 50-150 bases
602 of each other to increase the probability of fragment deletion.
603 DNA templates for CRISPR gRNAs were synthesized using plasmid pX335-U6-
604 Chimeric_BB-CBh-hSpCas9n(D10A) (Addgene, plasmid #42335; Cong et al., 2013)
605 containing the gRNA scaffold. The gRNA scaffold was amplified using a specific forward
606 primer for each gRNA, with an overhang containing the gRNA target sequence and T7
607 promoter, and a reverse primer that was identical for all reactions. For gRNAs that did not start
608 with G, an additional G was added at the start to ensure efficient transcription. The DNA
609 template was amplified using Q5 polymerase (New England Biolabs, NEB) and purified using
610 the Monarch PCR & DNA Cleanup Kit (NEB). The gRNAs were synthesized using the HiScribe
611 T7 High Yield RNA Synthesis Kit (NEB) and purified using the Monarch RNA Cleanup Kit
612 (NEB) and stored at -80°C before use. Alternatively, chemically modified synthetic gRNAs
613 were ordered directly from Synthego (CRISPRevolution sgRNA EZ Kit).
614
615 **Embryo injection**
616 On the day of injection, 1200 ng gRNA were mixed with 2400 ng Cas9 protein with NLS (PNA
617 Bio) in 5 µl nuclease-free water and incubated for 10 minutes at room temperature to form
618 ribonucleoprotein (RNP) complexes. For gRNA multiplexing, two RNP mixes were combined
619 1:1 to a final volume of 5 µl, and 0.5 µl of 10x 10,000 MW rhodamine dextran (Invitrogen)
620 added to better visualize the injection mixture. Injection mixtures were kept on ice throughout

621 the injection session. 50 µl glass microcapillaries (Drummond Microcaps) were pulled in a
622 capillary needle puller (PC-10, Narishige) set to 58°C with two light and one heavy weights, in
623 single-stage pulling mode. Fertilized sterlet eggs were manually dechorionated using Dumont
624 #5 forceps. A 1000 µl pipette tip cut to the same diameter as a dechorionated sterlet egg was
625 used to prepare a series of wells in an agar plate to allow ideal egg positioning during injection
626 using an automatic microinjector (FemtoJet 4x, Eppendorf), set to 100 hPa. Approximately 20
627 nl of the injection mixture (corresponding to approximately 4.8 ng gRNAs and 9.6 ng Cas9)
628 were injected into fertilized eggs or two-cell stage embryos, targeting the animal pole at a 45°
629 angle. Injected embryos were moved to a clean Petri dish and, for optimum Cas9 efficiency,
630 kept at room temperature until the end of the injecting session or until at least the 32-cell stage,
631 then moved to a 16°C incubator. No more than 30 eggs were kept per 90 mm Petri dish.
632 Unfertilized eggs and dead embryos were removed at the end of the injection day. Petri dishes
633 were checked regularly for dead embryos and the water was changed at least twice a day
634 before gastrulation was completed, and once daily post-gastrulation. Hatched larvae were
635 kept for approximately 16 days post fertilisation until stage 45, then euthanized by MS-222
636 overdose and fixed with modified Carnoy's fixative (see above). Fixed larvae were then
637 dehydrated stepwise into 100% ethanol and stored at -20°C.
638
639 **Gene cloning, *in situ* hybridization and immunohistochemistry**
640 Total RNA was isolated from sterlet embryos using Trizol (Invitrogen, Thermo Fisher
641 Scientific), following the manufacturer's protocol, and cDNA synthesized using the Superscript
642 III First Strand Synthesis kit (Invitrogen, Thermo Fisher Scientific). We used our sterlet
643 transcriptome assemblies (from pooled yolk-sac larvae at stages 40-45; preprint: Minařík et
644 al., 2023), which are available at DDBJ/EMBL/GenBank under the accessions
645 GKLU00000000 and GKEF01000000, to design primers for *Neurod4* (forward:
646 GAGAGAGCCCCAAAGAGACGAG; reverse: CTGCTTGAGCGAGAAGTTGACG). cDNA
647 fragments amplified under standard PCR conditions were cloned into the pDrive cloning vector
648 (Qiagen). Individual clones were verified by sequencing (Department of Biochemistry
649 Sequencing Facility, University of Cambridge, UK) and sequence identity verified using NCBI
650 BLAST (https://blast.ncbi.nlm.nih.gov/Blast.cgi; McGinnis and Madden, 2004). For *Neurod1*,
651 *Neurod2* and *Neurod6*, synthetic gene fragments based on sterlet transcriptome data, with
652 added M13 forward and reverse primer adaptors, were ordered from Twist Bioscience.
653 GenBank accession numbers are as follows: *Neurod1* OQ808944, *Neurod2* OQ808945,
654 *Neurod4* OQ808946, *Neurod6* OQ808947. The other genes used in this study have been
655 published (preprint: Minařík et al., 2023).
656 Digoxigenin-labelled riboprobes were synthesized as previously described (preprint:
657 Minařík et al., 2023). Whole-mount *in situ* hybridization (ISH) was performed as previously

658 described (Modrell et al., 2011a). Whole-mount immunostaining post-ISH for Sox2 (rabbit
659 monoclonal, 1:200; ab92494, Abcam) was performed as previously described (Metscher and
660 Müller, 2011), using a horseradish peroxidase-conjugated goat anti-rabbit antibody (1:300,
661 Jackson ImmunoResearch) and the metallographic peroxidase substrate EnzMet kit
662 (Nanoprobes) as per the manufacturer's instructions.
663
664 **Genotyping**
665 To confirm successful mutation in targeted regions, genotyping was performed on trunk and
666 tail tissue that had been removed before ISH and stored in 100% ethanol at -20°C. The tissue
667 was digested using Rapid Extract Lysis Kit (PCR Biosystems) and the target region amplified
668 using HS Taq Mix Red (PCR Biosystems) according to the manufacturer's instructions.
669 Primers used for genotyping are listed in Supplementary file 1. After agarose gel
670 electrophoresis, PCR products were extracted using MinElute Gel Extraction Kit (Qiagen) and
671 submitted for sequencing (Genewiz by Azenta Life Sciences). To analyze CRISPR editing
672 efficiency, Sanger trace files were uploaded to the Synthego Inference of CRISPR Edits (ICE)
673 tool (https://ice.synthego.com; Conant et al., 2022).
674
675 **Data availability statement**
676 The publication and associated supplementary figures include representative example images
677 of embryos from each experiment. Additional raw data underlying this publication consist of
678 further images of these and other embryos from each experiment. Public sharing of these
679 images is not cost-efficient but they are available from the corresponding author upon
680 reasonable request.
681
682 **Ethics statement**
683 Sterlet animal work was reviewed and approved by The Animal Research Committee of
684 Research Institute of Fish Culture and Hydrobiology, Faculty of Fisheries and Protection of
685 Waters, University of South Bohemia in České Budějovice, Vodňany, Czech Republic and
686 Ministry of Agriculture of the Czech Republic (MSMT-12550/2016-3).
687
688 **Author contributions**
689 CB conceived and designed the project and wrote the manuscript together with MM. MM
690 performed most of the experiments, prepared all the manuscript figures and made a significant
691 contribution to the writing of the manuscript. AC and RF performed some experiments. MV
692 made essential contributions to the experiments. MH provided draft genome sequence data.
693 MP and DG were instrumental in enabling all work with sterlet embryos. All authors read and
694 commented on the manuscript.

Funding

This work was supported by the Biotechnology and Biological Sciences Research Council (BBSRC: grant BB/P001947/1 to CB). Additional support for MM was provided by the Cambridge Isaac Newton Trust (grant 20.07[c] to CB) and by the School of the Biological Sciences, University of Cambridge. AC was supported by a PhD research studentship from the Anatomical Society. The work of RF and MP was supported by the Ministry of Education, Youth and Sports of the Czech Republic, projects CENAKVA (LM2018099), Biodiversity (CZ.02.1.01/0.0/0.0/16_025/0007370) and Czech Science Foundation (20-23836S).

Rights Retention Statement

This work was funded by a grant from the Biotechnology and Biological Sciences Research Council (BBSRC: BB/P001947/1). For the purpose of open access, the author has applied a Creative Commons Attribution (CC BY) licence to any Author Accepted Manuscript version arising.

Acknowledgements

Thanks to Melinda Modrell for pilot work on CRISPR/Cas9 in paddlefish and for her advice and helpful discussions in planning the project. Thanks to Marek Rodina and Martin Kahanec for their help with sterlet spawns. Thanks to David Jandzik, András Simon, Alberto Joven Araus, Ahmed Elewa, and Mustafa Khokha for invaluable advice on CRISPR/Cas9 approaches and genotyping. Thanks to Jan Stundl and David Jandzik for sharing their sterlet *Tyr* gRNA sequences prior to publication. Thanks to Christine Hirschberger and Rolf Ericsson for their help with some of the *in situ* hybridization rounds.

720 **References**

721 Anwar, M., Tambalo, M., Ranganathan, R., Grocott, T., Streit, A., 2017. A gene network
722 regulated by FGF signalling during ear development. Sci. Rep. 7, 6162.

723 Arendt, D., Musser, J.M., Baker, C.V.H., Bergman, A., Cepko, C., Erwin, D.H., Pavlicev, M.,
724 Schlosser, G., Widder, S., Laubichler, M.D., Wagner, G.P., 2016. The origin and
725 evolution of cell types. Nat. Rev. Genet. 17, 744-757.

726 Baker, C.V.H., 2019. The development and evolution of lateral line electroreceptors: insights
727 from comparative molecular approaches., in: B.A. Carlson, J.A. Sisneros, A.N. Popper,
728 R.R. Fay (Eds.), Electroreception: Fundamental Insights from Comparative Approaches.
729 Springer, Cham, pp. 25-62.

730 Baker, C.V.H., Modrell, M.S., 2018. Insights into electroreceptor development and evolution
731 from molecular comparisons with hair cells. Integr. Comp. Biol. 58, 329-340.

732 Baker, C.V.H., Modrell, M.S., Gillis, J.A., 2013. The evolution and development of vertebrate
733 lateral line electroreceptors. J. Exp. Biol. 216, 2515-2522.

734 Baloch, A.R., Franěk, R., Tichopád, T., Fučíková, M., Rodina, M., Pšenička, M., 2019. *Dnd1*
735 knockout in sturgeons by CRISPR/Cas9 generates germ cell free host for surrogate
736 production. Animals (Basel) 9, 174.

737 Bellono, N.W., Leitch, D.B., Julius, D., 2017. Molecular basis of ancestral vertebrate
738 electroreception. Nature 543, 391-396.

739 Bellono, N.W., Leitch, D.B., Julius, D., 2018. Molecular tuning of electroreception in sharks
740 and skates. Nature 558, 122-126.

741 Bermingham, N.A., Hassan, B.A., Price, S.D., Vollrath, M.A., Ben-Arie, N., Eatock, R.A.,
742 Bellen, H.J., Lysakowski, A., Zoghbi, H.Y., 1999. *Math1*: an essential gene for the
743 generation of inner ear hair cells. Science 284, 1837-1841.

744 Bodznick, D., Montgomery, J.C., 2005. The physiology of low-frequency electrosensory
745 systems, in: T.H. Bullock, C.D. Hopkins, A.N. Popper, R.R. Fay (Eds.), Electroreception.
746 Springer, New York, pp. 132-153.

747 Brown, T.L., Horton, E.C., Craig, E.W., Goo, C.E.A., Black, E.C., Hewitt, M.N., Yee, N.G., Fan,
748 E.T., Raible, D.W., Rasmussen, J.P., 2023. Dermal appendage-dependent patterning of
749 zebrafish *atoh1a*+ Merkel cells. eLife 12, e85800.

750 Bullock, T.H., Bodznick, D.A., Northcutt, R.G., 1983. The phylogenetic distribution of
751 electroreception: evidence for convergent evolution of a primitive vertebrate sense
752 modality. Brain Res. Rev. 287, 25-46.

753 Butts, T., Modrell, M.S., Baker, C.V.H., Wingate, R.J.T., 2014. The evolution of the vertebrate
754 cerebellum: absence of a proliferative external granule layer in a non-teleost ray-finned
755 fish. Evol. Dev. 16, 92-100.

Caprara, G.A., Peng, A.W., 2022. Mechanotransduction in mammalian sensory hair cells. Mol. Cell. Neurosci. 120, 103706.

Chagnaud, B.P., Wilkens, L.A., Hofmann, M., 2021. The ampullary electrosensory system –a paddlefish case study, in: B. Fritzsch (Ed.), The Senses: A Comprehensive Reference. Elsevier, pp. 215-227.

Chen, J., Wang, W., Tian, Z., Dong, Y., Dong, T., Zhu, H., Zhu, Z., Hu, H., Hu, W., 2018. Efficient gene transfer and gene editing in sterlet. Front. Genet. 9, 117.

Chen, Y., Gu, Y., Li, Y., Li, G.L., Chai, R., Li, W., Li, H., 2021. Generation of mature and functional hair cells by co-expression of *Gfi1*, *Pou4f3*, and *Atoh1* in the postnatal mouse cochlea. Cell Rep. 35, 109016.

Conant, D., Hsiau, T., Rossi, N., Oki, J., Maures, T., Waite, K., Yang, J., Joshi, S., Kelso, R., Holden, K., Enzmann, B.L., Stoner, R., 2022. Inference of CRISPR edits from Sanger trace data. CRISPR J. 5, 123-130.

Cong, L., Ran, F.A., Cox, D., Lin, S., Barretto, R., Habib, N., Hsu, P.D., Wu, X., Jiang, W., Marraffini, L.A., Zhang, F., 2013. Multiplex genome engineering using CRISPR/Cas systems. Science 339, 819-823.

Crampton, W.G.R., 2019. Electroreception, electrogenesis and electric signal evolution. J. Fish Biol. 95, 92-134.

Cunningham, F., Allen, J.E., Allen, J., Alvarez-Jarreta, J., Amode, M.R., Armean, I.M., Austine-Orimoloye, O., Azov, A.G., Barnes, I., Bennett, R., Berry, A., Bhai, J., Bignell, A., Billis, K., Boddu, S., Brooks, L., Charkhchi, M., Cummins, C., Da Rin Fioretto, L., Davidson, C., Dodiya, K., Donaldson, S., El Houdaigui, B., El Naboulsi, T., Fatima, R., Giron, C.G., Genez, T., Martinez, J.G., Guijarro-Clarke, C., Gymer, A., Hardy, M., Hollis, Z., Hourlier, T., Hunt, T., Juettemann, T., Kaikala, V., Kay, M., Lavidas, I., Le, T., Lemos, D., Marugán, J.C., Mohanan, S., Mushtaq, A., Naven, M., Ogeh, D.N., Parker, A., Parton, A., Perry, M., Piližota, I., Prosovetskaia, I., Sakthivel, M.P., Salam, A.I.A., Schmitt, B.M., Schuilenburg, H., Sheppard, D., Pérez-Silva, J.G., Stark, W., Steed, E., Sutinen, K., Sukumaran, R., Sumathipala, D., Suner, M.M., Szpak, M., Thormann, A., Tricomi, F.F., Urbina-Gómez, D., Veidenberg, A., Walsh, T.A., Walts, B., Willhoft, N., Winterbottom, A., Wass, E., Chakiachvili, M., Flint, B., Frankish, A., Giorgetti, S., Haggerty, L., Hunt, S.E., Ilsley, G.R., Loveland, J.E., Martin, F.J., Moore, B., Mudge, J.M., Muffato, M., Perry, E., Ruffier, M., Tate, J., Thybert, D., Trevanion, S.J., Dyer, S., Harrison, P.W., Howe, K.L., Yates, A.D., Zerbino, D.R., Flicek, P., 2022. Ensembl 2022. Nucleic Acids Res. 50, D988-D995.

Dettlaff, T.A., Ginsburg, A.S., Schmalhausen, O.I., 1993. Sturgeon Fishes: Developmental Biology and Aquaculture. Springer-Verlag, Berlin.

792 Dirksen, M.-L., Jamrich, M., 1995. Differential expression of *fork head* genes during early
793 *Xenopus* and zebrafish development. Dev. Genet. 17, 107-116.
794 Du, K., Stöck, M., Kneitz, S., Klopp, C., Woltering, J.M., Adolfi, M.C., Feron, R., Prokopov, D.,
795 Makunin, A., Kichigin, I., Schmidt, C., Fischer, P., Kuhl, H., Wuertz, S., Gessner, J.,
796 Kloas, W., Cabau, C., Iampietro, C., Parrinello, H., Tomlinson, C., Journot, L.,
797 Postlethwait, J.H., Braasch, I., Trifonov, V., Warren, W.C., Meyer, A., Guiguen, Y.,
798 Schartl, M., 2020. The sterlet sturgeon genome sequence and the mechanisms of
799 segmental rediploidization. Nat. Ecol. Evol. 4, 841-852.
800 Duggan, C.D., Demaria, S., Baudhuin, A., Stafford, D., Ngai, J., 2008. Foxg1 is required for
801 development of the vertebrate olfactory system. J. Neurosci. 28, 5229-5239.
802 Eagleson, G.W., Dempewolf, R.D., 2002. The role of the anterior neural ridge and *Fgf-8* in
803 early forebrain patterning and regionalization in *Xenopus laevis*. Comp. Biochem.
804 Physiol. B Biochem. Mol. Biol. 132, 179-189.
805 Elewa, A., Wang, H., Talavera-López, C., Joven, A., Brito, G., Kumar, A., Hameed, L.S.,
806 Penrad-Mobayed, M., Yao, Z., Zamani, N., Abbas, Y., Abdullayev, I., Sandberg, R.,
807 Grabherr, M., Andersson, B., Simon, A., 2017. Reading and editing the *Pleurodeles waltl*
808 genome reveals novel features of tetrapod regeneration. Nat. Commun. 8, 2286.
809 Fei, J.-F., Lou, W.P.-K., Knapp, D., Murawala, P., Gerber, T., Taniguchi, Y., Nowoshilow, S.,
810 Khattak, S., Tanaka, E.M., 2018. Application and optimization of CRISPR-Cas9-
811 mediated genome engineering in axolotl (*Ambystoma mexicanum*). Nat. Protoc. 13,
812 2908-2943.
813 Flowers, G.P., Timberlake, A.T., McLean, K.C., Monaghan, J.R., Crews, C.M., 2014. Highly
814 efficient targeted mutagenesis in axolotl using Cas9 RNA-guided nuclease.
815 Development 141, 2165-2171.
816 Gillis, J.A., Modrell, M.S., Northcutt, R.G., Catania, K.C., Luer, C.A., Baker, C.V.H., 2012.
817 Electrosensory ampullary organs are derived from lateral line placodes in cartilaginous
818 fishes. Development 139, 3142-3146.
819 Golson, M.L., Kaestner, K.H., 2016. Fox transcription factors: from development to disease.
820 Development 143, 4558-4570.
821 Hanashima, C., Li, S.C., Shen, L., Lai, E., Fishell, G., 2004. *Foxg1* suppresses early cortical
822 cell fate. Science 303, 56-59.
823 Hernández, P.P., Olivari, F.A., Sarrazin, A.F., Sandoval, P.C., Allende, M.L., 2007.
824 Regeneration in zebrafish lateral line neuromasts: expression of the neural progenitor
825 cell marker sox2 and proliferation-dependent and-independent mechanisms of hair cell
826 renewal. Dev. Neurobiol. 67, 637-654.

827 Hwang, C.H., Simeone, A., Lai, E., Wu, D.K., 2009. *Foxg1* is required for proper separation
828 and formation of sensory cristae during inner ear development. Dev. Dyn. 238, 2725-
829 2734.
830 Iyer, A.A., Groves, A.K., 2021. Transcription factor reprogramming in the inner ear: turning on
831 cell fate switches to regenerate sensory hair cells. Front. Cell. Neurosci. 15, 660748.
832 Iyer, A.A., Hosamani, I., Nguyen, J.D., Cai, T., Singh, S., McGovern, M.M., Beyer, L., Zhang,
833 H., Jen, H.I., Yousaf, R., Birol, O., Sun, J.J., Ray, R.S., Raphael, Y., Segil, N., Groves,
834 A.K., 2022. Cellular reprogramming with ATOH1, GFI1, and POU4F3 implicate
835 epigenetic changes and cell-cell signaling as obstacles to hair cell regeneration in
836 mature mammals. eLife 11, e79712.
837 Jen, H.-I., Singh, S., Tao, L., Maunsell, H.R., Segil, N., Groves, A.K., 2022. GFI1 regulates
838 hair cell differentiation by acting as an off-DNA transcriptional co-activator of ATOH1,
839 and a DNA-binding repressor. Sci. Rep. 12, 7793.
840 Jørgensen, J.M., 2005. Morphology of electroreceptive sensory organs, in: T.H. Bullock, C.D.
841 Hopkins, A.N. Popper, R.R. Fay (Eds.), Electroreception. Springer, New York, pp. 47-
842 67.
843 Kawauchi, S., Santos, R., Kim, J., Hollenbeck, P.L.W., Murray, R.C., Calof, A.L., 2009. The
844 role of *Foxg1* in the development of neural stem cells of the olfactory epithelium. Ann.
845 N. Y. Acad. Sci. 1170, 21-27.
846 Kniss, J.S., Jiang, L., Piotrowski, T., 2016. Insights into sensory hair cell regeneration from
847 the zebrafish lateral line. Curr. Opin. Genet. Dev. 40, 32-40.
848 Leitch, D.B., Julius, D., 2019. Electrosensory transduction: comparisons across structure,
849 afferent response properties, and cellular physiology., in: B.A. Carlson, J.A. Sisneros,
850 A.N. Popper, R.R. Fay (Eds.), Electroreception: Fundamental Insights from Comparative
851 Approaches. Springer, Cham, pp. 63-90.
852 Lenhardt, M., Finn, R.N., Cakic, P., Kolarevic, J., Krpocetkovic, J., Radovic, I., Fyhn, H.J.,
853 2005. Analysis of the post-vitellogenic oocytes of three species of Danubian
854 Acipenseridae. Belg. J. Zool. 135, 205.
855 Lukoseviciute, M., Gavriouchkina, D., Williams, R.M., Hochgreb-Hagele, T., Senanayake, U.,
856 Chong-Morrison, V., Thongjuea, S., Repapi, E., Mead, A., Sauka-Spengler, T., 2018.
857 From pioneer to repressor: bimodal foxd3 activity dynamically remodels neural crest
858 regulatory landscape *in vivo*. Dev. Cell 47, 608-628.
859 Lush, M.E., Diaz, D.C., Koenecke, N., Baek, S., Boldt, H., St Peter, M.K., Gaitan-Escudero,
860 T., Romero-Carvajal, A., Busch-Nentwich, E.M., Perera, A.G., Hall, K.E., Peak, A., Haug,
861 J.S., Piotrowski, T., 2019. scRNA-Seq reveals distinct stem cell populations that drive
862 hair cell regeneration after loss of Fgf and Notch signaling. eLife 8, e44431.

McGinnis, S., Madden, T.L., 2004. BLAST: at the core of a powerful and diverse set of sequence analysis tools. Nucleic Acids Res. 32, W20-5.

Metscher, B.D., Müller, G.B., 2011. MicroCT for molecular imaging: quantitative visualization of complete three-dimensional distributions of gene products in embryonic limbs. Dev. Dyn. 240, 2301-2308.

Millimaki, B.B., Sweet, E.M., Dhason, M.S., Riley, B.B., 2007. Zebrafish *atoh1* genes: classic proneural activity in the inner ear and regulation by Fgf and Notch. Development 134, 295-305.

Minařík, M., Modrell, M.S., Gillis, J.A., Campbell, A.S., Fuller, I., Lyne, R., Micklem, G., Gela, D., Pšenička, M., Baker, C.V.H., 2023. Identification of multiple transcription factor genes potentially involved in the development of electrosensory versus mechanosensory lateral line organs. bioRxiv https://www.biorxiv.org/content/10.1101/2023.04.14.536701v1

Modrell, M.S., Baker, C.V.H., 2012. Evolution of electrosensory ampullary organs: conservation of *Eya4* expression during lateral line development in jawed vertebrates. Evol. Dev. 14, 277-285.

Modrell, M.S., Bemis, W.E., Northcutt, R.G., Davis, M.C., Baker, C.V.H., 2011a. Electrosensory ampullary organs are derived from lateral line placodes in bony fishes. Nat. Commun. 2, 496.

Modrell, M.S., Buckley, D., Baker, C.V.H., 2011b. Molecular analysis of neurogenic placode development in a basal ray-finned fish. genesis 49, 278-294.

Modrell, M.S., Lyne, M., Carr, A.R., Zakon, H.H., Buckley, D., Campbell, A.S., Davis, M.C., Micklem, G., Baker, C.V.H., 2017a. Insights into electrosensory organ development, physiology and evolution from a lateral line-enriched transcriptome. eLife 6, e24197.

Modrell, M.S., Tidswell, O.R.A., Baker, C.V.H., 2017b. Notch and Fgf signaling during electrosensory versus mechanosensory lateral line organ development in a non-teleost ray-finned fish. Dev. Biol. 431, 48-58.

Mogdans, J., 2019. Sensory ecology of the fish lateral-line system: Morphological and physiological adaptations for the perception of hydrodynamic stimuli. J. Fish Biol. 95, 53-72.

Moser, T., Grabner, C.P., Schmitz, F., 2020. Sensory processing at ribbon synapses in the retina and the cochlea. Physiol. Rev. 100, 103-144.

Mukhopadhyay, M., Pangrsic, T., 2022. Synaptic transmission at the vestibular hair cells of amniotes. Mol. Cell. Neurosci. 121, 103749.

Nicolson, T., 2017. The genetics of hair-cell function in zebrafish. J. Neurogenet. 31, 102-112.

Northcutt, R.G., 1997. Evolution of gnathostome lateral line ontogenies. Brain Behav. Evol. 50, 25-37.

899 Northcutt, R.G., Catania, K.C., Criley, B.B., 1994. Development of lateral line organs in the
900 axolotl. J. Comp. Neurol. 340, 480-514.
901 O'Neill, P., McCole, R.B., Baker, C.V.H., 2007. A molecular analysis of neurogenic placode
902 and cranial sensory ganglion development in the shark, *Scyliorhinus canicula*. Dev. Biol.
903 304, 156-181.
904 Papalopulu, N., Kintner, C., 1996. A posteriorising factor, retinoic acid, reveals that
905 anteroposterior patterning controls the timing of neuronal differentiation in *Xenopus*
906 neuroectoderm. Development 122, 3409-3418.
907 Pauley, S., Lai, E., Fritzsch, B., 2006. *Foxg1* is required for morphogenesis and histogenesis
908 of the mammalian inner ear. Dev. Dyn. 235, 2470-2482.
909 Pickett, S.B., Raible, D.W., 2019. Water waves to sound waves: using zebrafish to explore
910 hair cell biology. J. Assoc. Res. Otolaryngol. 20, 1-19.
911 Piotrowski, T., Baker, C.V.H., 2014. The development of lateral line placodes: Taking a
912 broader view. Dev. Biol. 389, 68-81.
913 Roccio, M., Senn, P., Heller, S., 2020. Novel insights into inner ear development and
914 regeneration for targeted hearing loss therapies. Hear. Res. 397, 107859.
915 Singh, S., Groves, A.K., 2016. The molecular basis of craniofacial placode development.
916 WIREs Dev. Biol. 5, 363-376.
917 Square, T., Romášek, M., Jandzik, D., Cattell, M.V., Klymkowsky, M., Medeiros, D.M., 2015.
918 CRISPR/Cas9-mediated mutagenesis in the sea lamprey *Petromyzon marinus*: a
919 powerful tool for understanding ancestral gene functions in vertebrates. Development
920 142, 4180-4187.
921 Square, T.A., Jandzik, D., Massey, J.L., Romášek, M., Stein, H.P., Hansen, A.W.,
922 Purkayastha, A., Cattell, M.V., Medeiros, D.M., 2020. Evolution of the endothelin
923 pathway drove neural crest cell diversification. Nature 585, 563-568.
924 Stundl, J., Soukup, V., Franěk, R., Pospisilova, A., Psutkova, V., Pšenička, M., Cerny, R.,
925 Bronner, M.E., Medeiros, D.M., Jandzik, D., 2022. Efficient CRISPR mutagenesis in
926 sturgeon demonstrates its utility in large, slow-maturing vertebrates. Front. Cell Dev.
927 Biol. 10, 750833.
928 Tasdemir-Yilmaz, O.E., Druckenbrod, N.R., Olukoya, O.O., Dong, W., Yung, A.R., Bastille, I.,
929 Pazyra-Murphy, M.F., Sitko, A.A., Hale, E.B., Vigneau, S., Gimelbrant, A.A.,
930 Kharchenko, P.V., Goodrich, L.V., Segal, R.A., 2021. Diversity of developing peripheral
931 glia revealed by single-cell RNA sequencing. Dev. Cell 56, 2516-2535.
932 Toresson, H., Martinez-Barbera, J.P., Bardsley, A., Caubit, X., Krauss, S., 1998. Conservation
933 of *BF-1* expression in amphioxus and zebrafish suggests evolutionary ancestry of
934 anterior cell types that contribute to the vertebrate telencephalon. Dev. Genes Evol. 208,
935 431-439.

936 Uribe-Salazar, J.M., Kaya, G., Sekar, A., Weyenberg, K., Ingamells, C., Dennis, M.Y., 2022.
937 Evaluation of CRISPR gene-editing tools in zebrafish. BMC Genomics 23, 12.
938 Webb, J.F., 2021. Morphology of the mechanosensory lateral line system of fishes, in: B.
939 Fritzsch (Ed.), The Senses: A Comprehensive Reference. Elsevier, pp. 29-46.
940 Whitear, M., 1989. Merkel cells in lower vertebrates. Arch. Histol. Cytol. 52 Suppl., 415-422.
941 Wu, X., Kriz, A.J., Sharp, P.A., 2014. Target specificity of the CRISPR-Cas9 system. Quant.
942 Biol. 2, 59-70.
943 York, J.R., Zehnder, K., Yuan, T., Lakiza, O., McCauley, D.W., 2019. Evolution of Snail-
944 mediated regulation of neural crest and placodes from an ancient role in bilaterian
945 neurogenesis. Dev. Biol. 453, 180-190.
946 Yu, H.V., Tao, L., Llamas, J., Wang, X., Nguyen, J.D., Trecek, T., Segil, N., 2021. POU4F3
947 pioneer activity enables ATOH1 to drive diverse mechanoreceptor differentiation through
948 a feed-forward epigenetic mechanism. Proc. Natl. Acad. Sci. U.S.A. 118, e2105137118.
949 Zhang, S., Zhang, Y., Dong, Y., Guo, L., Zhang, Z., Shao, B., Qi, J., Zhou, H., Zhu, W., Yan,
950 X., Hong, G., Zhang, L., Zhang, X., Tang, M., Zhao, C., Gao, X., Chai, R., 2019.
951 Knockdown of *Foxg1* in supporting cells increases the trans-differentiation of supporting
952 cells into hair cells in the neonatal mouse cochlea. Cell. Mol. Life Sci. 77, 1401-1419.
953 Zhang, Y., Zhang, S., Zhang, Z., Dong, Y., Ma, X., Qiang, R., Chen, Y., Gao, X., Zhao, C.,
954 Chen, F., He, S., Chai, R., 2020. Knockdown of *Foxg1* in Sox9+ supporting cells
955 increases the trans-differentiation of supporting cells into hair cells in the neonatal mouse
956 utricle. Aging (Albany NY) 12, 19834-19851.
957 Zhao, X.-F., Suh, C.S., Prat, C.R., Ellingsen, S., Fjose, A., 2009. Distinct expression of two
958 *foxg1* paralogues in zebrafish. Gene Expr. Patterns 9, 266-272.
959

960

Target gene	sgRNA	Target sequence	PAM	Combinations used
Tyr	1	GGTGCCAAGGCAAAAACGCT	GGG	1+2, 1+2+3+4
	2	GATATCCCTCCATACATTAT	TGG	1+2, 1+2+3+4
	3	GATGTTTCTAAACATTGGGG	TGG	1+2+3+4
	4	GCTATGAATTTATTTTTTTC	AGG	1+2+3+4
	5	GCAAGGTATACGAAAGTTGA	CGG	5+6
	6	GATTGCAAGTTCGGCTTCTT	TGG	5+6
	7*	GGTTAGAGACTTTATGTAAC	GGG	7+8
	8*	GGCTCCATGTCTCAAGTCCA	AGG	7+8
Atoh1	1	GACCTTGTAAAAGATCGGAA	AGG	1+2
	2	GCTTGTCATTGTCAAATGAC	GGG	1+2
Neurod4	1	GGAGCGTTTCAAGGCCAGGC	GGG	1, 1+2+3+4, 1+6
	2	GTGAGCGTTCTCGCATGCAC	GGG	2, 1+2+3+4
	3	GCCTGGCCCACAACTACATC	TGG	1+2+3+4, 3+4+5+6
	4	GAGGGGCCCCGAGAAGCTGC	AGG	1+2+3+4, 3+4+5+6
	5	GTCTCCCCAGCCCTCCCTAC	GGG	5, 3+4+5+6
	6	GACAACCACTCCCCGGATTG	CGG	1+6, 3+4+5+6
	7	GACCCTGCGCAGGCTCTCCA	GGG	7+9, 7+8+9
	8	GCAGCTGGGTCCCCTGCTGA	CGG	7+8+9
	9	GGGGCCGTGTGCTCAGGGAT	GGG	7+9, 7+8+9
Foxg1	1	GAAACATCTTTTGCCCAACC	CGG	1+2
	2	TCTTCCGAGCAAGGTAACTC	GGG	1+2
	3	TGATGCTGAAGGACGACTTG	GGG	3+4
	4	CTGGCTCGTCCTCGGGCCGG	TGG	3+4

961

962 **Table 1. sgRNAs used in this study.** List of the genes targeted for CRISPR/Cas9-mediated
963 mutagenesis, together with the target sequences and combinations of sgRNAs reported in this
964 study. *Note:* Tyr sgRNAs 7 and 8 (marked with an asterisk) were designed and recently
965 published by Stundl et al. (2022) as their *tyr* sgRNA 3 and *tyr* sgRNA 4, respectively.